Heliyon 10 (2024) e38966

Contents lists available at ScienceDirect

Heliyon

journal homepage: www.cell.com/heliyon

Research article

Ferritin adsorption onto chrysotile asbestos fibers influences the protein secondary structure

Martina Zangari [a,b], Federica Piccirilli [c,d], Lisa Vaccari [d], Cristian Radu [e], Paola Zacchi [f], Annalisa Bernareggi [f], Sara Leone [g], Giuliano Zabucchi [f,*], Violetta Borelli [f,**]

[a] Department of Physics, University of Trieste, 34127, Trieste, Italy
[b] CERIC-ERIC, S.S. 14 - km 163,5, 34149, Basovizza, Trieste, Italy
[c] Area Science Park, Padriciano 99, 34149, Trieste, Italy
[d] Elettra Sincrotrone Trieste, S.S. 14 - km 163,5, 34149, Basovizza, Trieste, Italy
[e] National Institute of Materials Physics, Atomistilor 405A, 077125, Magurele, jud. Ilfov, Romania
[f] Department of Life Science, University of Trieste, via via Valerio 28-28/1, 34127, Trieste, Italy
[g] Fiber laboratory, Azienda Sanitaria Giiuliano Isontina (ASUGI), Trieste, Italy

ARTICLE INFO

Keywords:
Asbestos fibers
Iron
Holo-ferritin
Apo-ferritin

ABSTRACT

Asbestos fiber exposure triggers chronic inflammation and cancer. Asbestos fibers can adsorb different types of proteins. The mechanism of this adsorption, not yet completely understood, has been studied in detail mainly with serum albumin and was shown to induce structural changes in the bound protein. The findings of these works regarded mainly the changes of the protein structure, independently of any relation with asbestos-related diseases. For the first time, we have focused our attention to the consequences of the interaction between asbestos fibers and ferritin, a protein involved in iron metabolism, which is strongly modified in asbestos-related diseases. Even if it is known that ferritin can be adsorbed by asbestos fibers, the results of this interaction for the ferritin secondary structure has not previously been studied. One consequence of asbestos-ferritin interaction, is the formation of the so-called ferruginous/asbestos bodies (ABs). In the AB-coating material, the secondary structure of ferritin is modified, and at present, it is unclear whether or not this modification is a direct consequence of the asbestos interaction. In the present study, chrysotile asbestos, more than other asbestos fiber types tested, was found to rapidly bind holo-ferritin, and the presence of iron seemed to play a key role in this process, since iron-free apo-ferritin was adsorbed at a lower level, and iron-saturated chrysotile lost its ferritin-adsorbing capacity. To directly study the details of ferritin adsorption on asbestos fibers, High Resolution Transmission Electron Microscopy (HR-TEM) was employed together with FTIR micro-spectroscopy and Infrared nanoscopy, which to the best of our knowledge, have not previously been used for this purpose. Chrysotile-bound apo-ferritin underwent a significant change in secondary structure, showing a shift from a prevalent α-helix to a β-sheet conformation. Conversely, the adsorbed holo-ferritin structure appeared to be only weakly modified. These findings add a new potential mechanism to the toxic activities of asbestos: the fibers can modify

* Corresponding author.
** Corresponding author.
E-mail addresses: martina.zangari@units.it (M. Zangari), federica.piccirilli@areasciencepark.it (F. Piccirilli), lisa.vaccari@elettra.eu (L. Vaccari), cristian.radu@infim.ro (C. Radu), pzacchi@units.it (P. Zacchi), abernareggi@units.it (A. Bernareggi), sara.leone@asugi.sanita.fvg.it (S. Leone), zabucchi@units.it (G. Zabucchi), borelliv@units.it (V. Borelli).

https://doi.org/10.1016/j.heliyon.2024.e38966
Received 1 October 2024; Accepted 3 October 2024
Available online 4 October 2024

the structure, and very likely, the function of adsorbed proteins. This, in relation to ferritin, could be a key mechanism in cell iron homeostasis alteration, typically reported in asbestos-related diseases.

1. Introduction

Asbestos fiber exposure triggers chronic inflammation of the lungs, known as asbestosis, and tumor development. While the chronic inflammation soon follows the cytotoxic effect of the fibers, the neoplastic transformation, which shows a long-lasting latency time [1], also requires genetic mutations and growth advantage [2]. Two of the major malignant diseases associated with asbestos exposure are malignant pleural mesothelioma (MPM) and lung cancer (LC) [3–5]. Even though the exact mechanisms responsible for the lung and pleural cell injury, as well as those involved in the development of the related diseases, are still largely unclear, they seem to be dependent on Reactive Oxygen Species (ROS) production [6–8]. In this context, the iron content of the fibers could be a key factor in determining their toxicity, due to its known capacity to trigger the production of ROS [8,9]. However, numerous other factors may contribute to asbestos toxicity, such as direct cell membrane piercing or the capacity to adsorb different proteins and thereby affect their function [10–15].

The commercial term "asbestos" refers to some fibrous mineral silicates, divided into two groups: the serpentine, including chrysotile (Chry), and amphiboles, including among others, amosite (Amo) and crocidolite (Croc) [16,17]. It has been reported that each type of fiber adsorbs a different profile of proteins, suggesting specific adsorption mechanisms [18–20]. Moreover, alterations of both structure and function of the adsorbed protein are suggested to be a possible consequence of these interactions [10,19–25]. In line with this concept, some mastocyte and leukocyte granule components, such as chymase and eosinophil peroxidase, improve their enzymatic activity after binding Croc [10].

A well-known example of protein-asbestos fiber interaction is provided by asbestos bodies formation (ABs), also known as ferruginous/asbestos bodies. These peculiar structures are usually made of an asbestos fiber, either amphiboles or serpentine, coated with mucopolysaccharides and iron-containing proteins [26,27]. Their count is one of the tools to assess the degree of asbestos fiber exposure for legal actions [28,29]. The fiber coating has been suggested to represent a protective mechanism, initiated by macrophages, in an attempt to segregate the cytotoxic fibers from the biological tissues [30]. More recently, our group and other authors [30–33], have suggested that the coating material itself could maintain, and even enhance, the cytotoxic and pro-inflammatory properties of asbestos by favoring the generation of ROS and stimulating inflammatory cells. Indeed, the surface iron of ABs was found to be catalytically active [34,35]. Naturally-occurring compounds such as citrate, ascorbate and adenosine diphosphate (ADP) can promote ferrous iron mobilization at physiological concentrations from Amo and Croc [36], ferric iron can be released from Amo at acidic pH [37] and surface ferric iron can be released from Chry [38]. Shen and colleagues [39] also showed that Croc and Amo can adsorb ferric iron at slightly alkaline or acidic pH. This evidence altogether supports the idea that asbestos fibers can either adsorb or release iron depending on their chemical structure and surrounding conditions.

The presence of ferritin in the AB coating material has been convincingly reported [33,40] together with a misfolded secondary structure of the protein [41]. Once the asbestos fibers reach the cell interior, either by direct membrane piercing or by phagocytic ingestion [10–15], they, under favorable conditions, could affect iron homeostasis by adsorbing ferritin, and releasing/adsorbing iron ions [21,25,41–43], and also by exerting ferrous iron oxidizing activity [44]. Through a still unknown mechanism, the cells could eventually respond to asbestos exposure triggering a significant new ferritin synthesis [45,46], which suggests an imbalance between ferritin availability and free iron. In line with this idea, an overload of iron and ferritin, has been found in respiratory cells exposed to asbestos, despite an increased expression of the divalent metal transporter-1 (DMT1). This evidence has been confirmed in *in vitro* and animal model studies, as well as in tissues derived from exposed patients [47–50]. This complex scenario, which suggests a functional iron deficiency in the presence of iron overload, is the result of excess iron being sequestered and thus no longer available, that paradoxically leads the cell to seek for it. Eventually, the fiber inside the cells may undergo AB formation, following ferritin sequestration, from which the release of iron could be irreversibly impaired. Altogether, this evidence strongly links asbestos pathogenicity to alteration of iron homeostasis. It also suggests that the interaction of the fibers with ferritin may allow a long-lasting ROS-mediated cytotoxic activity through iron overload and AB activity [33]. To these events, a chronic inflammatory reaction, a good favorable ground for genetic mutations, can ensue.

Here, the possible structural modification directly induced by interaction of ferritin with asbestos fibers was investigated, taking advantage of an *in vitro* AB model, where the pure protein interacts with the fibers under conditions that mimic the intracellular milieu (*e.g.* cytosol and phagosome). The adsorption and structural modifications of the iron-loaded ferritin (holo-ferritin, HoloF) and its iron-free form (apo-ferritin, ApoF) upon asbestos fiber interaction, were investigated by the synergic interplay of ultraviolet (UV) spectroscopy, Fourier transform infrared (FTIR), high resolutiom transmission electron microspectroscopy (HR-TEM) and infrared nanoscopy.

The obtained results suggest a novel asbestos fiber activity, capable in principle, of affecting the iron homeostatic mechanisms of exposed cells.

2. Materials and methods

2.1. Reagents

Pure proteins and chemicals: holo-ferritin (HoloF) and apo-ferritin (ApoF) from horse spleen, tris (hydroxymethyl) amino methane (TRIS), PBS, KCl, NaCl and NaOH were purchased from Sigma-Aldrich.

Fibers: Analytical Standard UICC samples of Crocidolite, Amosite and Chrysotile were purchased from SPI-CHEM, West Chester, PA, USA. The reference batches of the standard samples were: crocidolite (Croc) South Africa (CAS 02704-AB); chrysotile (Chry) A Rhodesian, (CAS 02701-AB) and amosite (Amo) (CAS 02703-AB). Standard fibers used in this project spanned from 0.5 to 100 μm in length and from 0.1 to 1.2 μm in width [51]. Dry asbestos fibers were handled in a hood Multihazard Glovebox to prevent inhalation at Azienda Sanitaria Universitaria Giuliano-Isontina (ASUGI). For the following experiments, asbestos fibers were first re-suspended by a qualified operator in phosphate buffered saline (PBS) at a final concentration of 10 mg/mL, and stored at 4 °C until use (mother solution). Before each experiment, the mother solution was left to sediment for 2 min before taking a definite aliquot for the following experimental steps, to avoid large fiber aggregates.

2.1.1. Fiber saturation with iron (III)

2 mg/mL of Chry fibers were saturated with $Fe_2(SO_4)_3$ 1 mM in TRIS buffer 20 mM pH 7.0 at room temperature (RT) for 2 h under continuous mixing in a wheel. After the incubation, the Chry suspension was centrifuged at 10,000 rpm for 10 min to separate the pellet and the supernatant. After three washings in 0.9 % NaCl, the pellet appeared yellow (See Fig. 1S suggesting iron enrichment). The iron-rich fibers were resuspended, at the same concentration, in 0.9 % NaCl and the amount of Fe^{3+} adsorbed was calculated following the method described in Zangari et al. [44]; it was ~2.5 nmoles of Fe^{3+}per μg of Chry.

2.1.2. Incubation protocols for the preparation of protein-fiber adducts

For the preparation of the protein-fiber adducts, ferritins HoloF and ApoF, were incubated with asbestos fibers following the protocol developed by Valerio *et al* [18], adapted to our specific system, described as follows: after incubation for a fixed time, according to Protocol 1 or 2 as specified in the following, the suspension was centrifuged at 10,000 rpm for 10 min in an Eppendorf microcentrifuge. The pellets, made of proteins, which interact with fibers resulting in adducts assembling, were resuspended in 0.9 % NaCl and stored at 4 °C. The supernatants, composed mainly of proteins that did not interact with fibers and not-pelleted smaller fibers, were picked up and stored at 4 °C. The protein-fiber adducts were prepared at pH 5.0 and pH 7.0 in order to mimic the cell environments encountered after fiber inhalation and cell ingestion [52]. Two types of incubation protocols were followed, as follows:

Protocol 1: pure HoloF and ApoF were incubated with 1 mg of Chry fibers at RT in TRIS buffer 20 mM (pH 7.0) or acetate buffer 20 mM (pH 5.0), in a final volume of 1 mL at different concentrations (from 200 μg/mL to 1000 μg/mL) for 5, 10, 30, 60 and 120 min under continuous mixing in the wheel at RT to avoid fiber precipitation. The final concentrations considered, expressed in weight ratio (w:w), relative to concentration of the fiber (1 mg/mL), were: 0.2, 0.4, 0.6, 0.8, 1. The same protocol was used for ferritin-fiber adduct formation with Amo and Croc, with the sole exception that just a single weight fraction, 0.4 w:w, and a fix time, 120 min, was used. The aforementioned ferritin-fiber adducts were used for dose calibration, time and fiber specificity analysis and also for the preparation of the samples for infrared nanoscopy measurements. The extent of ferritin absorption onto fibers was evaluated by electrophoresis (Sodium Dodecyl Sulfate PolyAcrylamide Gel Electrophoresis SDS-PAGE) and by UV spectrophotometry (PerkinElmer lambda 25). For SDS-PAGE, the pellets were washed twice in 0.9 % NaCl and the bound proteins were extracted by boiling for 15 min in 0.4 mL of NaOH 0.3 M, SDS 1 % and analyzed.

The concentration of ferritin solutions was determined by spectrophotometric analysis, by recording UV spectra at 280 nm against a blank buffer solution. The measurements were performed using a 1 cm quartz cell. The amount of adsorbed protein was calculated as the difference between the concentrations of the initial solution and that of the supernatant (tenfold diluted) after solid separation. The calibration curves are plotted in Fig. 2S. The figure shows that at the two different pHs used, in the range of concentrations employed (5–80 μg/mL), the increase of absorbance was linear with increasing protein concentration. This allowed us to calculate the amount of ferritin sequestered by the fibers on the basis of the optical density (OD) decrease in the remaining supernatant following fiber-protein complexes centrifugation.

Protocol 2: the incubation of pure ApoF and HoloF with Chry at a weight ratio of 0.4 w:w was performed in four different solutions, 1–2: in a KCl:KOH solution 68 mM, pH 5.0 (phagosome late) and pH 7.0 (phagosome early), mimicking the phagosome environment [53,54] and 3: in a KCl:KOH solution 120 mM pH 5.0 and 7.0, for mimicking the cytosolic environment [52,53] and 4: in a KCl:KOH solution 120 mM pH 5.0, that does not represent a physiological relevant environment, while it allowed us to better discriminate the effect of pH and salinity on protein adsorption. The incubation was performed at three fixed times: 2 h, 48 h and 1 week. The incubation temperature was set to 37 °C and the incubation was performed under mixing (Thermomixer Comfort Eppendorf) at 800 rpm to avoid fiber precipitation. The aforementioned Ferritin:Fiber adducts were used for protein secondary structure analysis by FTIR microspectroscopy and for HR-TEM imaging.

2.1.3. Fourier transform infrared microspectroscopy (Micro-FTIR): data acquisition and analysis

The Ferritin-Chry adducts were prepared according to Protocol 2. Measurements were performed on Ferritin-Chry adducts resuspended in 0.9 % NaCl and cytocentrifuged on the CaF_2 window. Briefly, 250 μL of Ferritin-Chry adducts solutions were dropped in a funnel for cytocentrifuge and they were cytocentrifuged for 10 min in Cytospin 2 (Shandon Inc) at 500 rpm on CaF_2 slides, 0.5 mm thick and with a diameter of 10 mm. To match the cytospin standard sample holder, a custom-made silicon support was used to mount

CaF_2 slides on a conventional microscopic slide. The compact layer of Ferritin-Chry adducts obtained through cytocentrifugation guaranteed the non-volatility of the fibers and excellent spectral quality. IR adsorption micro-spectra were measured at SISSI-Bio infrared beamline of Elettra Sincrotrone Trieste [55]. Micro-FTIR was performed with the in-vacuum Vertex70v interferometer coupled to the Hyperion 3000 microscope. A conventional thermal source (Globar) and a Mercury Cadmium Telluride (MCT) detector working at a 40 kHz were used. The measurements were performed in transmission mode, using a condenser/objective pair 15×/15×. A measurement area of 50 × 50 μm^2 was set to select randomized sample regions in order to avoid saturation. 1024 scans at 4 cm^{-1} spectral resolution were averaged in order to optimize the signal to noise ratio (S/N) according to the samples' optical characteristics. At least 50 points per sample were acquired. Spectra were corrected for atmospheric adsorption, and a baseline was subtracted by using a Rubberband correction algorithm [56] with the OPUS PRO 7.5 software (Bruker Optics, Ettlingen, Germany). Qualitative information on the protein secondary structure was determined from 2nd-derivative analysis of the Amide I adsorption band (1600–1700 cm^{-1}). To this aim, 15 absorbance spectra were first averaged upon normalization on to the fiber bands in the 832-1138 cm^{-1} spectral region and then the second derivative procedure with 13-points smoothing filter was applied. The Amide I normal mode of vibration is mainly to peptide-backbone C=O stretching (~80 % of the mode) and N–H bending (~20 % of the mode) adsorptions and it is highly sensitive to protein structural changes [57].

2.1.4. ATR-FTIR measurements

Attenuated Total Reflection Fourier Transform Infrared (ATR-FTIR) measurements of the pristine proteins and supernatant of Ferritin-Chry adducts were performed using a nitrogen-purged Vertex70 interferometer (Bruker Optics, Ettlingen, Germany) equipped with a thermal source (Globar) and a deuterated triglycine sulfate (DTGS) detector at SISSI-Bio infrared beamline of Elettra Sincrotrone Trieste [55]. The single reflection ATR accessory by PIKE with diamond Internal Reflection Element (IRE) was used. Briefly, pure HoloF and ApoF were incubated for 2 h, 48 h, and 1 week in solution mimicking the cytosol (120 mM KCl, pH 7.0, 37 °C) and phagosome (68 mM KCl, pH 7.0 and 5.0, 37 °C) under continuous mixing (Protocol 2). After the incubation time, the proteins were centrifuged at 10,000 rpm for 10 min and stored at 4 °C. 5 μL of these solutions were dropped onto the IRE and measured after complete drying under gentle nitrogen flux. The supernatants obtained according to Protocol 2 were measured following the same sampling approach. Measurements were acquired with a scanner velocity of 5 kHz in the spectral range 400–4000 cm^{-1} by averaging 256 scans. Spectra were corrected for atmospheric contribution, and a baseline was subtracted by using a Rubberband correction algorithm. Second-derivative analysis was performed, applying a 9-points smoothing filter. Data acquisition and processing were performed using OPUS PRO 7.5 software (Bruker Optics, Ettlingen, Germany).

2.1.5. Infrared nanoscopy

The vibrational analysis at the nanoscale of pristine fibers and Ferritin-Chry adducts was done taking advantage of infrared nanoscopy. To this aim, 5 μL of samples, prepared according to Protocol 1, were dropped onto gold-coated Si wafers and then allowed to dry into a closed dish. The samples were then washed three times with Milli-Q water to remove the excess of NaCl salt crystals and measured after complete drying. Only a few, tightly bound fibers remained anchored onto the substrate. The measurements were carried out at the SISSI-Bio infrared beamline of Elettra Sincrotrone Trieste [55,58] by exploiting the Neascope microscope by Attocube System AG, equipped with a scattering-type Scanning Near field Optical Microscopy (SNOM) module, for spectroscopy measurements, and a imaging module, for Pseudo Heterodyne, PsHet. imaging. Arrow type, high sensitivity, tips with a diameter of 20 nm and coated with PtIr (Neaspec GmbH, Munich) were used in order to collect the scattered IR signal. The microscope was operated in tapping mode with the cantilever oscillating at a frequency of 235 kHz with a free amplitude around 100 nm. The DFG (Difference Frequency Generation) laser chip delivering light in the spectral region 1000-2000 cm^{-1}, with maximum emission at 1666 cm^{-1} was used for spectroscopy measurements in order to probe protein modes (Amide I at 1580-1710 cm^{-1} and Amide II at 1480-1580 cm^{-1}). Spectra were acquired at a resolution of 8 cm^{-1} with each measurement taking around 3 min. A clean gold surface was used as a reference in order to calculate IR absorbance. A Quantum Cascade Laser (QCL) was conversely used for image acquisition exploiting the imaging module. Neaplot (Attocube System AG, Munich) software was used for spectroscopic data analyses and topographic imaging maps were analyzed with Gwyddion 2.59. The images were built up by considering the 3rd-harmonic and the 4th-harmonic of the optical signal in order to compare the absorption of the samples at different penetration depths, being the first more penetrating than the latter, in a penetration range not exceeding 100 nm for the 2nd-harmonic of the signal [59,60].

2.1.6. High-Resolution Transmission Electron Microscopy (HR-TEM)

To better understand the adsorption of ferritin onto the asbestos fibers, HR-TEM experiments were carried out at the National Institute of Material Physics, BUCHAREST-MAGURELE Laboratory of Atomic Structures and Defects in Advanced Materials in Bucharest (NIMP, CERIC-ERIC facility). HR-TEM images were acquired using the atomic resolution analytical JEOL JEM ARM200F microscope operated at 200 KV and equipped with a JEOL JED-2300 T unit for Energy-Dispersive X-Ray spectroscopy (EDS) analysis. The samples were observed in conventional TEM (CTEM).

3. Results and discussion

3.1. Ferritin interactions with asbestos fibers

For the purpose of our studies, a simplified *"in vitro"* model was exploited, composed of pure HoloF and ApoF adsorbed onto asbestos fibers, referred from here on as protein-fiber adducts. Firstly, with the aim of setting the optimal experimental conditions for

adducts formation, the extent of HoloF adsorption on 0.5–1.0 mg/mL Chry was evaluated after 2 h of incubation at room temperature (RT). In these preliminary experiments, the same amount of protein (0.110 ± 0.010 μg protein/μg fibers) was adsorbed, independently on the protein concentrations (*e.g.* from 400 to 600 μg/mL, $n = 4$), revealing an excess of protein with respect to the adsorption capacity of the fibers. Thus, the following experiments were performed using a fiber concentration of 1.0 mg/mL and a protein concentration of 400 μg/mL, unless otherwise indicated. When the adsorbing capacity of different fiber types was analyzed, the extent of HoloF adsorption on Chry reached a value of 0.108 ± 0.018 μg protein/μg fibers ($n = 10$), while in the case of Croc and Amo the values were 0.045 ± 0.0012 ($n = 3$) and 0.021 ± 0.0025 ($n = 3$) μg/μg fibers, respectively. As shown in Fig. 1a, these values were significantly different (Chry *vs* Cro, $^{***}P < 0.001$, Chry *vs* Amo, $^{**}P = 0.01$). Having shown that Chry was able to bind ferritin to a higher extent with respect to the other types of asbestos fibers, we decided to focus our study on the Chry-Ferritin interaction. The dose-response curve in Fig. 1b, shows that at 400 μg/mL of protein, 0.121 ± 0.019 μg/μg fibers ($n = 3$) were adsorbed as a maximum value, confirming the above observations. The time course of formation of the HoloF -Chry adducts is shown in Fig. 1c. The adduct formation kinetics were quite fast since ~80 % of the maximum adsorption value was already reached after 10 min, while the plateau was reached after 30 min. A different adsorbing capacity of Chry has been reported also for other proteins, such as bovine serum albumin (BSA); in this case, Chry was found to bind more proteins (*e.g.* 0.009 μg BSA/μg fibers) than Croc (*e.g.* 0.003 μg BSA/μg fibers) [18]. Interestingly, the values were about 13.4 times and 3.3 times lower than those we found for HoloF.

These results suggest that a wide spectrum of interactions, in relation to both fiber and protein types, are involved in the adducts formation, as also suggested by other authors [19,21]. Subsequently, the extent of adsorption of HoloF and ApoF on Chry was compared at pHs similar to those encountered inside the macrophages (*e.g.* cytosol: 7.0; phagosome early: 7.0, and phagosome late: 5.0) [52], the first cell-type that comes in contact with the fibers. Holoferritin and newly synthesized apoferritin are cytosolic proteins. When the stored iron of holoferritin is required for cellular functions (*e.g.* in macrophages), it must be released from the protein. For this purpose, holoferritin enters an autophagocytic process, known as ferritinophagy, where, following the proteinases activity at low pH, the proteins are digested and iron is made free [61]. Therefore, holo/apo ferritins are found both in the cytosolic and in the phagolysosomal compartment. On the other hand, the fibers can be found either in the cytosol (entering by cell membrane piercing) or into the phagosome (entering by ingestion) [10,12,13]. The result is that fibers and ferritins can meet in these two compartments. Accordingly, we tested the ferritin-chrysotile adsorption at either pH 5.0 (phagosome) or 7.0 (cytosol and phagosome early). As summarized in Fig. 2a, Chry bound ApoF significantly less than HoloF at pH 7.0 ($^{**}P < 0.01$). Conversely, at pH 5.0, the difference in adsorption was not significant. The difference between HoloF and ApoF adsorption at pH 7.0 was further confirmed by SDS-PAGE analysis on the pellets collected after centrifuging the protein-fiber mixture (Fig. 2b). Of note, the high variability, of either

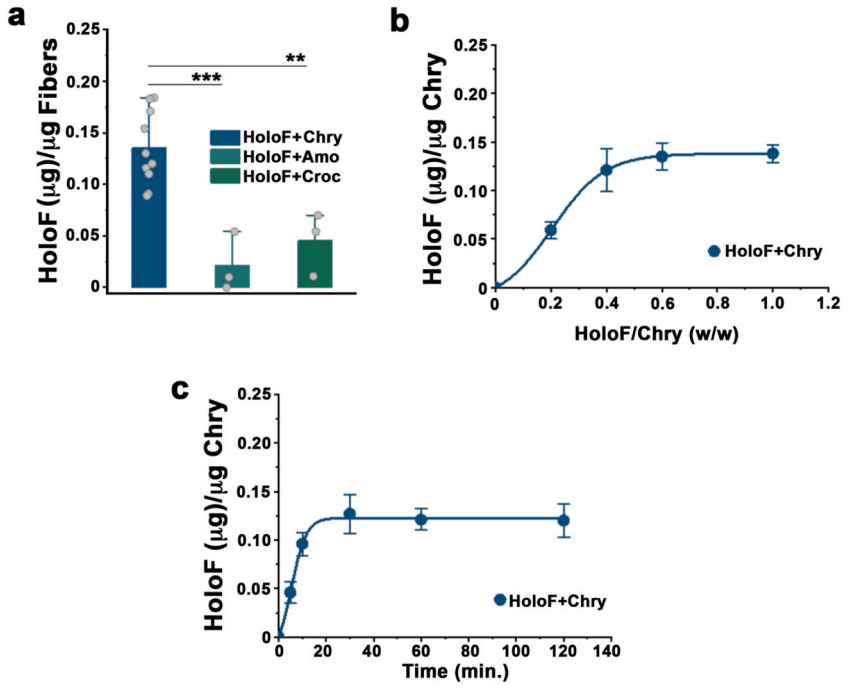

Fig. 1. *Optimization of the experimental conditions for setting up protein:fiber adducts.* **a**) HoloF adsorption on different types of asbestos fibers in TRIS buffer (20 mM pH 7.0). UV–Vis data. Amount of HoloF (400 μg) adsorbed onto 1 mg of fibers; final volume 1 mL. Chry ($n = 10$); Cro ($n = 3$) and Amo ($n = 3$). HoloF was adsorbed more significantly onto Chry *vs* Croc ($^{***}P < 0.001$) and *vs* Amo ($^{**}P < 0.001$) fibers. One-Way ANOVA (with Tukey's post hoc). **b**) Dose-response curve for HoloF adsorption onto Chry fibers. UV–Vis data. At plateau (400 μg), 0.121 ± 0.019 (mean ± SE) μg were found adsorbed on 1 μg of fibers ($n = 3$). Fiber concentration = 1 mg, final volume = 1 mL. **c**) Time course of HoloF adsorption onto Chry fibers. UV–Vis data. Note that ~80 % of the maximum value was reached after 10 min of incubation. HoloF 400 μg, Chry 1 mg ($n = 3$), final volume 1 mL.

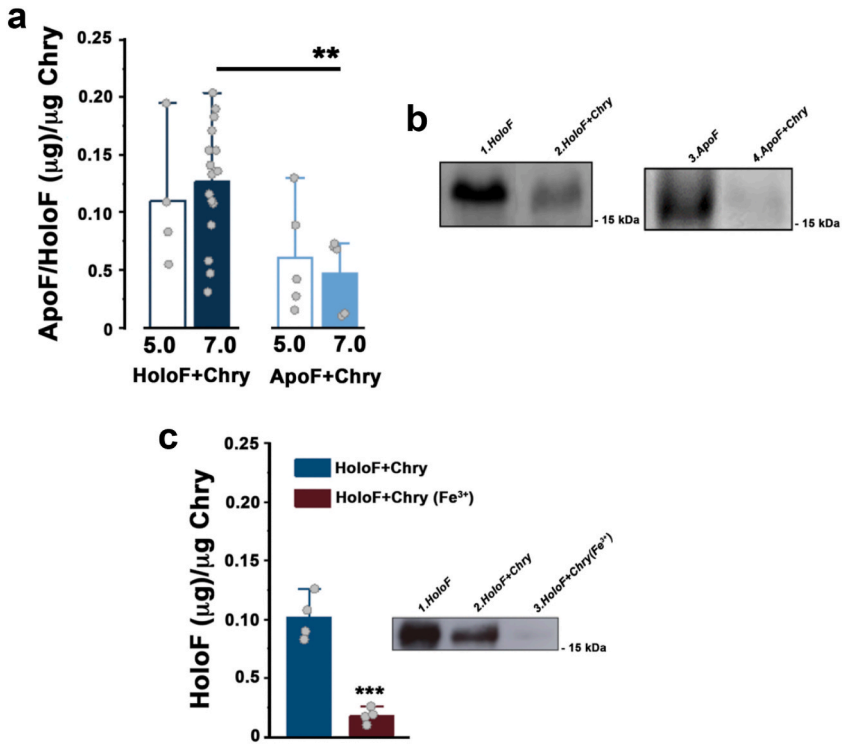

Fig. 2. *Adsorption of ferritin isoforms onto chrysotile: effect of pH and iron-saturation* **a**) Amount of HoloF and Apo-F adsorption onto Chry at different pHs. TRIS 20 mM, pH 7.0 and acetate 20 mM pH 5.0). Protein concentration 400 μg, Chry 1 mg; final volume 1 mL. Uv–Vis data. The amount of HoloF adsorbed was not significantly different at the pHs tested (pH 7.0 $n = 16$, pH 5.0 $n = 4$). HoloF adsorption was significantly higher with respect to ApoF at pH 7.0 (**$P < 0.01$, unpaired t-test). Values are means ± SE. **b**) SDS-PAGE showing that ApoF was bound at a lower extent (lane 4) with respect to the iron-loaded counterpart (lane 2). In lanes 1 and 3 the protein inputs are shown. **c**) HoloF absorption on iron-doped Chry; protein concentration 400 μg, Chry 1 mg; final volume 1 mL. UV–Vis data. Values are the mean ± SE of 4 exps (***$P < 0.0001$, t-test, $n = 4$). **Inset** SDS-PAGE: lane 1, HoloF input (20 μg protein); lane 2, 50 μL of the protein extract obtained from the adduct HoloF:Chry; lane 3, 50 μL of the protein extract obtained from the adduct HoloF:iron-doped Chry. All samples were boiled for 5 min in 1 % SDS. Coomassie stained. See Materials and Methods for details.

holoferritin or apoferritin adsorption may be explained by the heterogeneity of this phenomenon. This can be easily revealed by the ultrastructural appearance of the adducts (see below). The complexity of adduct formation was confirmed by the finding that HoloF and ApoF were adsorbed similarly at pH 7.0 and 5.0. HoloF and ApoF share a similar isoelectric point (IP), 4.1–5.1 and thus, at pH 7.0, they are both negatively charged and can bind by electrostatic interaction the positively charged Chry fibers (IP = 10). Assuming a pure electrostatic interaction, a reduced adsorption is expected at pH 5.0. Since this is not the case, the involvement of other weak interactions *e.g.* H-bonds affecting the adsorption capacity, has to be taken into consideration [9,21].

The lower extent of adsorption of the iron-free protein ApoF by the iron-poor Chry fibers, suggests that iron may play some role in the protein-fiber interaction mechanism. Iron-saturated Chry tended to remain yellow-coloured, even after extensive washing (Fig. 1S), as a consequence of a direct and persistent iron binding, as reported also by others [21,25,41–43]. Moreover, the supernatant analysis by UV (Fig. 2c) and the SDS-PAGE of the pellets (*inset* in Fig. 2c) revealed a strong inhibition of HoloF adsorption onto these iron-enriched Chry fibers. This intriguing role of iron would also explain the reason why Croc and Amo (iron-rich fibers) adsorb less HoloF. A similar effect has been reported for BSA, in which the amount of protein adsorbed on iron-doped synthetic Chry was found to decrease when the iron increased [22]. In this case, as a result of the iron doping extent, the metal could replace both Mg and Si of Chry, modifying the structure of the fiber [22]. Similar changes of iron-saturated Chry structure could have some role in the HoloF-fiber interaction, and thus explain its failure in adsorbing HoloF. We speculate that during the Chry-HoloF interaction, the iron of the protein may interact with the fiber and stabilize the HoloF-fiber interaction. This aspect deserves to be investigated in the future. We did not further investigate the mechanism of chrysotile-ferritin adduct formation. It may include electrostatic bonds, protein charge density, hydrogen bond formation and hydrophobic effects. Moreover, the combination of these bonds could be specific for each type of protein [22,62]. Also this subject deserves to be investigated in the future. Here, we focused mainly on ferritin secondary structure under conditions of optimal interaction. On this note, for detaching the proteins from fibers, a strong treatment was required: extensive washing in 0.9 % NaCl and 15 min boiling in NaOH and SDS. Thus, apart from the chemical nature of the Ferritin-Chry interaction, the strength of their binding seems to be very strong. In line with this observation, a large amount of ferritin has been detected in the coating material of ABs only after strong treatment [33]. Accordingly, it is likely that the ferritin-sequestration can hinder a functional participation, either of AB-associated ferritin or of ferritin in Ferritin-Chry adducts, in the cell iron homeostatic process.

3.2. Nanoscale morphochemical characterization of HoloF - and ApoF-Chry adducts

In order to better investigate the morphochemical characteristics of HoloF-Chry and ApoF-Chry adducts, HR-TEM and infrared nanoscopy were exploited. HR-TEM analyses focused on the models more relevant from a biological perspective, *i.e.* HoloF-Chry and ApoF-Chry adducts at cytosolic conditions (pH 7.0, KCl 120 mM), incubated for 2 and 48 h. HR-TEM images acquired on the HoloF - and ApoF-Chry adducts are presented in Fig. 3. HoloF-Chry adducts (Fig. 3 panels a–c) showed the presence of electron-dense roundish structures having a diameter of ~6 nm in all tested conditions (**panels a-b**). These structures are commonly observed by TEM when HoloF is imaged and correspond to the iron core of HoloF [63]. As expected, at high magnification (**panel c**), these structures showed the presence of a crystal structure, compatible with the typical appearance of ferrihydrite, the main component of the ferritin iron core [64]. The electron-dense structures were closely related to the fiber as a homogeneous monolayer of single molecules (**inset in panel a**). However, frequently, the ferritin adsorption was not homogeneous and appeared to accumulate at specific sites on the fibers, which may express a different chemical composition favoring the adsorption (Fig. 3 panel b). Interestingly, at these sites, the ferritin molecules adsorbed onto the fiber seemed to bind in turn, more ferritin, forming a bulge on the fiber. Even if we cannot exclude that some pre-aggregated ferritin molecules could have been involved, the observation that these bulges were observed on either site of the fiber (arrowheads in panel **b**) makes this possibility unlikely. A heterogeneous adsorption of ferritin and the variability seen in Fig. 2a may be the basis of the peculiar asbestos body structures [65]. Fig. 3a and b shows that one fiber can bind holoferritin heterogeneously, even if a homogeneous layer is the main pathway of adsorption; frequently, an accumulation of bound molecules is seen. Also, some fibers appear to bind holoferritin to a weak extent. Even if we used UICC standard chrysotile, we cannot be sure to employ amounts of fibers with the same binding capacity.

No significant morphological differences were found between the appearance of HoloF-adducts in cytosolic or phagosomal conditions, either sampled at 2 or 48 h (data not shown). Fig. 3 (panels d, e) shows the ultrastructural appearance of ApoF-Chry adducts. In

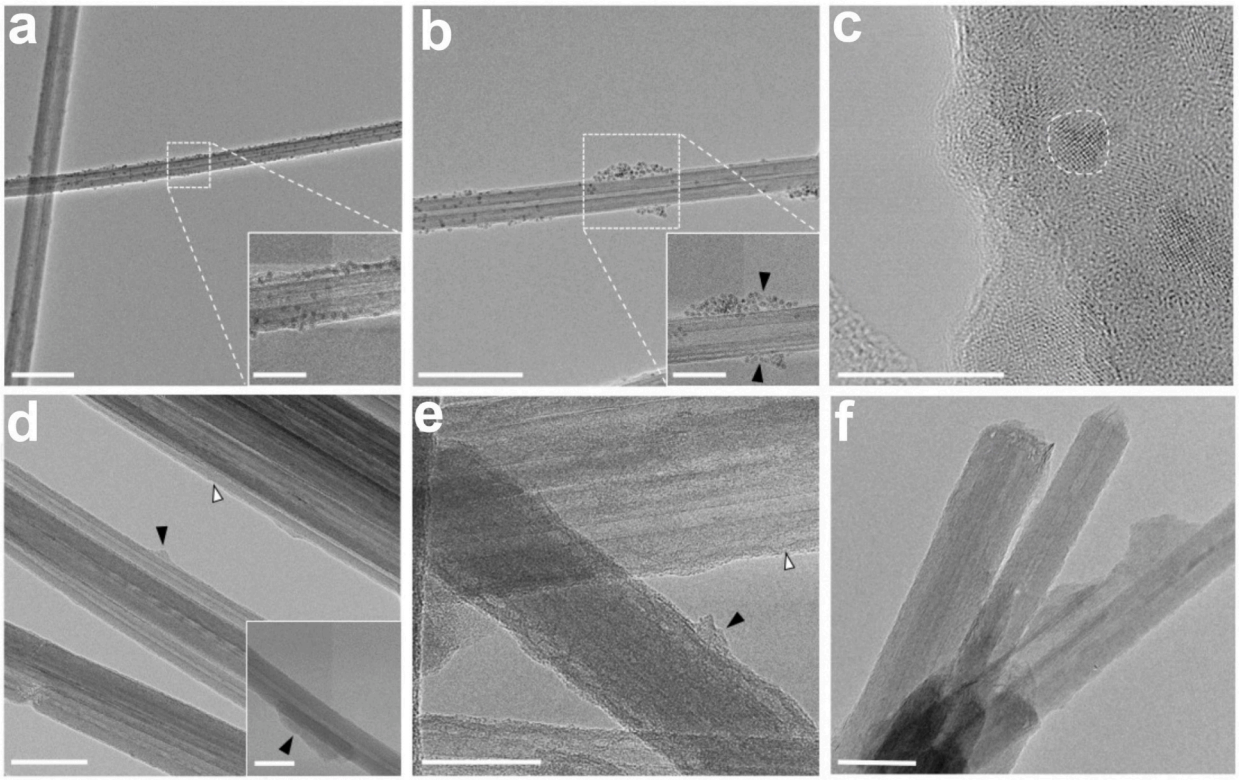

Fig. 3. *HR-TEM images of HoloF-Chry adducts*. In panels **a-c**, the ultrastructure of HoloF-Chry adducts formed in cytosolic conditions is shown. No significant morphological difference was found between the appearance of HoloF-adducts in either cytosolic or phagosomal conditions or sampled at 2 and 48 h. Roundish electrodense structures are clearly evident for each imaged condition. They formed a continuous monolayer or accumulated in a bulge. In panel **c**, crystal structures (*e.g.* that enclosed in a dotted line) compatible with that of ferrihydrite are evident. The ultrastructural appearance of ApoF-Chry adducts is shown in panels **d** and **e**. In all the tested conditions, the fibers were coated with a non-electron dense layer a few nanometers thick (white arrowheads in panel **d** and **e**) that appeared more homogenous and regular with respect to that observed for HoloF-Chry. This amorphous layer was not formed when the fiber was incubated without proteins in the cytosol-mimicking solution. Also, for ApoF-Chry adducts, the coating layer was not always homogeneous and sometimes formed bulges (black arrowheads in panels **d** and **e**). HR-TEM image of Chry fibers after 48 h of incubation in cytosolic-mimicking solution is also shown for comparison (panel **f**). Scale bars: 200 nm in panel **a** and **b**; 100 nm in panels **d;** in all the insets and panel **f,** 50 nm; 10 nm in panel **c**.

all the tested conditions, the fibers were coated with a non-electron dense layer a few nanometers thick that appeared more homogenous and regular (black arrowheads in **panels d and e)** with respect to that observed for HoloF -Chry. This amorphous layer was not formed when the fiber was incubated without proteins in the cytosol mimicking solution. Also, for ApoF-Chry adducts, the coating layer was not always homogeneous and sometimes formed bulges (white arrowheads in **panels d and e)**. Again, no significant morphological difference was found between the samples in all the tested conditions (data not shown). An HR-TEM image of Chry fibers after 48 h of incubation in cytosolic-mimicking solution is also reported for comparison **(panel f).**

In order to add chemical information at the nanoscale to the results already obtained with HR-TEM, and especially on the material adherent onto the fiber surface, infrared nanoscopy was exploited. In Fig. 4, panels **a** and **e,** the AFM topography of HoloF-Chry and ApoF-Chry adducts upon 2 h of incubation at cytosolic pH is shown. The nano-FTIR absorbance spectrum collected on the surface of the HoloF-Chry adduct in the 1750-1450 cm^{-1} spectral region, plotted in Fig. 4 panel **b**, clearly shows the Amide I and Amide II bands of proteins and demonstrates that HoloF is bound to Chry. The same considerations can be drawn for the ApoF-Chry adduct: the nano-FTIR absorbance spectrum exhibited the presence of Amide I and II peaks (see Fig. 4, panel **f**), indicating that ApoF is also adsorbed onto the fiber. For comparison purposes, panels **i** and **j** of Fig. 4 show AFM topography and the nano-FTIR absorbance spectrum in the 1750-1450 cm^{-1} spectral region of a raw Chry fiber upon 2 h incubation in cytosolic conditions without the presence of ferritin. The absorbance spectrum did not show any relevant spectral feature, excluding possible spectral interference of the fiber with the nano-FTIR absorbance spectra of the adducts. Overall, the results highlight that the low electron density material which decorates asbestos fibers revealed by HR-TEM analysis is made of ferritin, and further confirms that the electron-dense roundish structures are indeed the HoloF metallic core. In addition, the IR images at 1640 cm^{-1} revealed a uniform distribution of both HoloF (panels **c** and **d,** third and

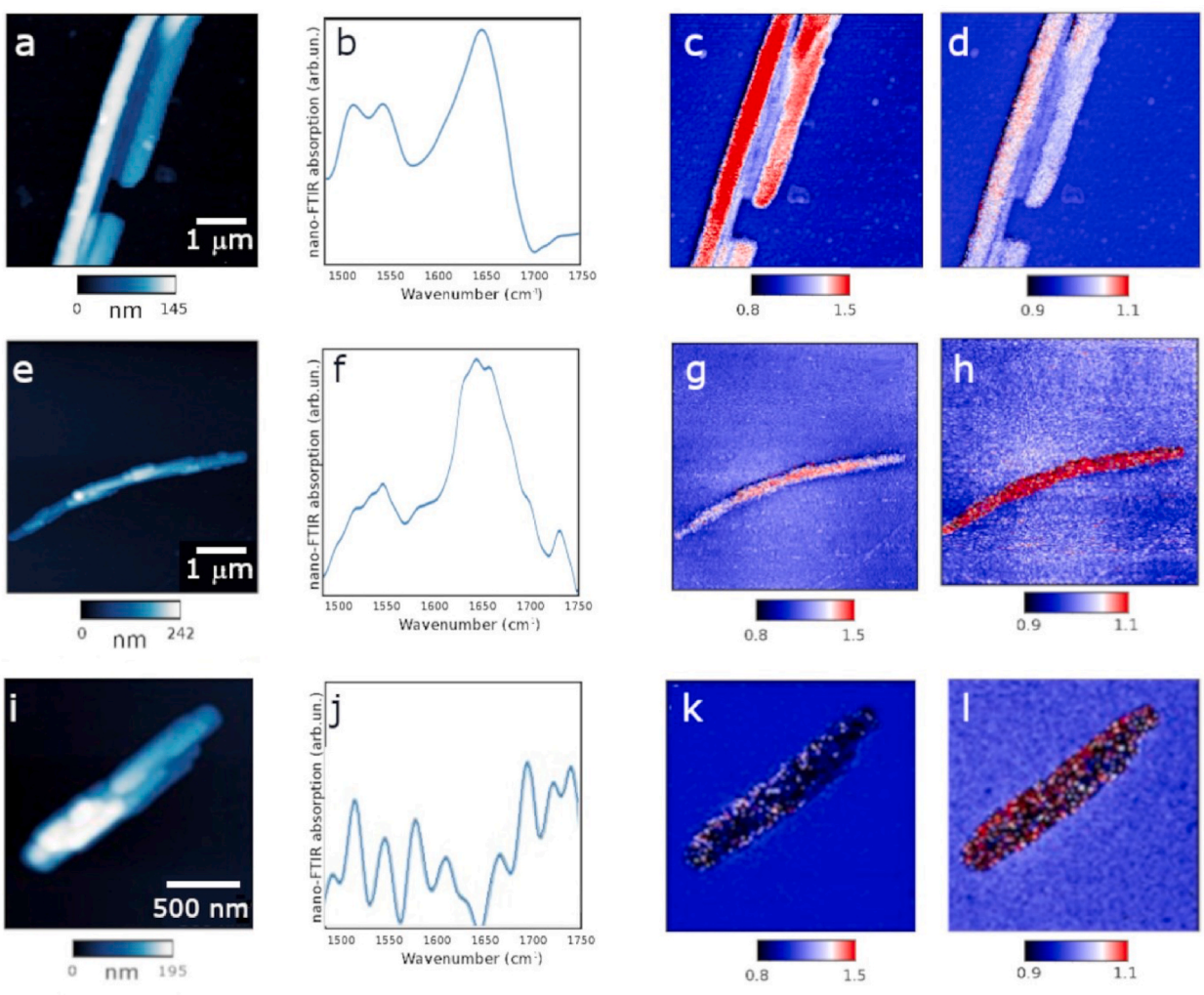

Fig. 4. *IR nanoscopy of HoloF- and ApoF-Chry adducts*. (**a**, **e**, **i**) AFM topography of HoloF-Chry, ApoF-Chry and raw Chry fiber respectively. (**b**, **f**, **j**) nano-FTIR absorbance spectrum in the 1750-1450 cm^{-1} spectral region of HoloF-Chry, ApoF-Chry and raw Chry fiber respectively. (**c**, **g**, **k**) nano-IR chemical image at 1640 cm^{-1}, third harmonic of the signal (O3P) of HoloF-Chry, ApoF-Chry and raw Chry fiber respectively. (**d**, **h**, **l**) nano-IR chemical image at 1640 cm^{-1}, fourth harmonic of the signal (O4P) of HoloF-Chry, ApoF-Chry and raw Chry fiber respectively.

fourth harmonic of the optical signal respectively) and ApoF (panel **g** and **h,** third and fourth harmonic of the optical signal respectively) across the surface of Chry. Since the penetration depth of the fourth harmonic is smaller than the third [60], by analyzing the different contrast for HoloF and ApoF adducts, it can be inferred that ApoF is mainly loaded onto the fiber surface, while HoloF seems more intimately bound into the fiber. For ApoF, the third harmonic protein signal was "diluted" into the background, while becoming more clearly detectable over the background at the fourth harmonic of the signal. Conversely, the fainter fourth harmonic signal of HoloF, with respect to the third, can be interpreted as a deeper penetration of the protein into the fiber structure. As already highlighted, it is indeed known that HoloF and ApoF have the same net charge, but the iron core of HoloF determines a redistribution of the surface charges of the protein and major conformational flexibility [66,67]. Despite accessing the same binding sites, HoloF and ApoF may locally interact differently with the fiber, thereby explaining their penetration capacity and potential impact on their structure. Again, the presence of iron induces a more intimate interaction and may possibly affect the fiber structure.

3.3. HoloF and ApoF secondary structure on protein-chry adducts

To assess and follow in time, the possible secondary structure rearrangements of HoloF and ApoF occurring after the formation of the adduct, micro-FTIR experiments were performed. In an attempt to approximate in the best possible manner, the biological environment encountered by the asbestos fibers following cell ingestion/penetration, the adducts were assembled in KCl salt to mimic the saline concentrations of cytosolic and phagosome compartments, aiming to create an environment that more closely resembles the *in vivo* conditions. In particular, potassium ions (K^+) are the most abundant in the inner compartments of cells, and chloride ions (Cl^-)

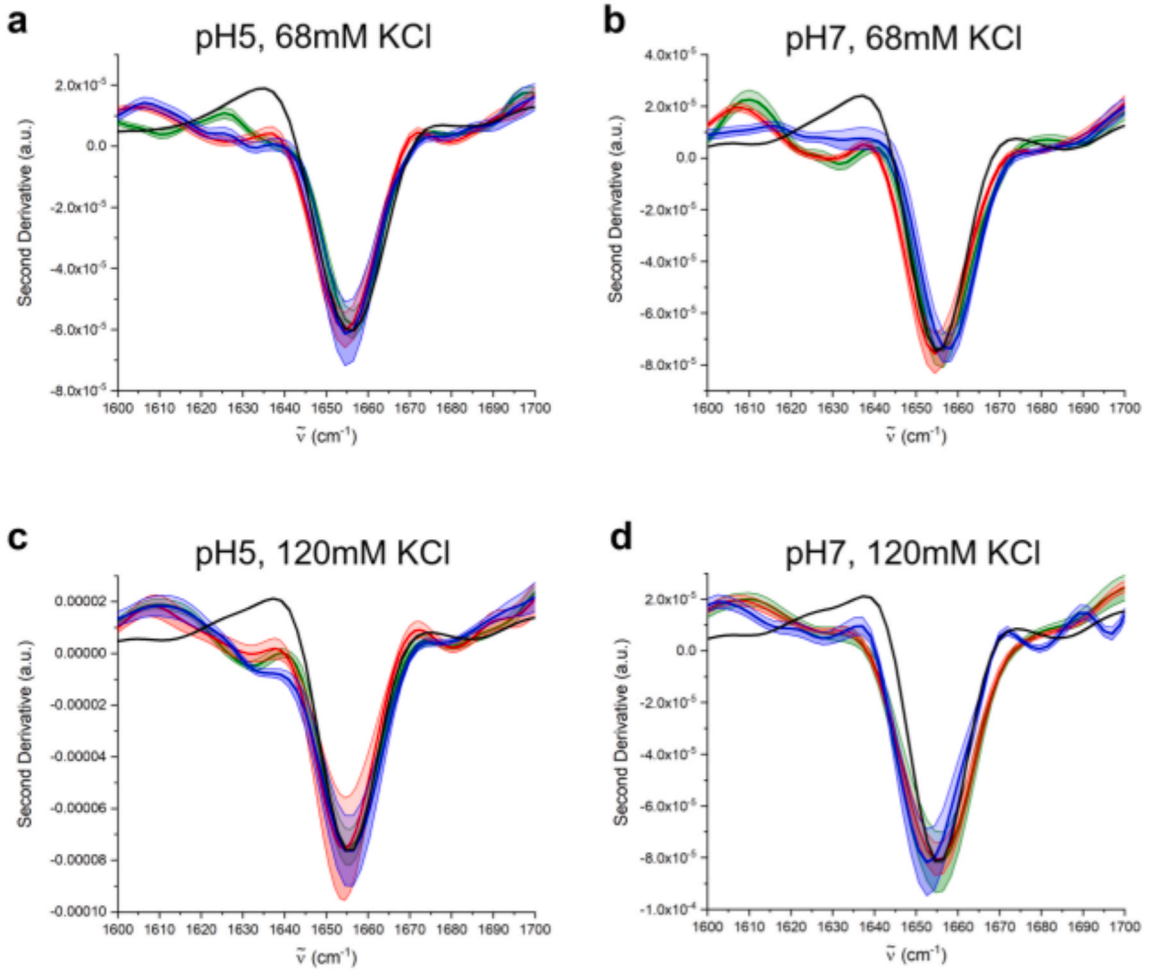

Fig. 5. *Micro-FTIR spectra of HoloF-Chry adducts*. Second derivative of HoloF-Chry adduct micro-spectra averaged on fifteen acquisitions at incubation times 2 h (green plot), 48 h (red line) and 1 week (blue line) for the following incubation conditions: **a**) 68 mM KCl, pH 5 (phagosomal conditions); **b**) 68 mM KCl, pH 7.0 (phagosomal conditions); **c**) 120 mM KCl, pH 5.0 (cytosolic conditions); **d**) 120 mM KCl, pH 7.0 (cytosolic conditions). Green, red and blue-shadowed regions represent the spectral standard deviation at each considered incubation time. HoloF second derivative ATR-FTIR spectrum is also plotted for each pH and ionic strength (black line). Data are normalized at the main peak. The helix pattern (1656 cm^{-1}) of HoloF loaded on Chry, when compared to pristine HoloF, is well preserved for all tested conditions. For more details see text.

are crucial for modulating ion strength and pH. Moreover, both ions are involved in bacterial killing activity within the phagosome. The protein-fiber interaction was therefore investigated in both cytosolic conditions, at pH 7.0, 120 mM KCl, 37 °C, and in phagosomal conditions, at pH 5.0 and pH 7.0, 68 mM KCl, 37 °C. An additional condition was introduced into the study, which is not biologically relevant: the F-Chry adduct assembled at 120 mM KCl and pH 5.0. This approach enabled us to disentangle the specific influences of pH and ionic strength on the adsorption process and facilitate a meaningful parallel analysis between phagosome and cytosol conditions. Having previously verified that the complete uptake of ferritin on Chry occurs in less than 1 h (see Fig. 1b), the incubation time was set to 2 h, 48 h and 1 week. Figs. 5 and **6** show the second derivative spectra of HoloF -Chry and ApoF-Chry adducts in the Amide I region (1600–1700 cm^{-1}) for all the aforementioned conditions. The spectra of the adducts were compared to the ones of pristine HoloF and ApoF incubated under the same experimental conditions for the longest incubation time, 1 week.

It is relevant at this stage, to highlight that the spectral contribution of the fiber in the Amide I spectral region was negligible and did not affect the spectral analysis on the protein secondary structure that followed. For more information, see Fig. 3S panel b. Second derivative spectra of pristine HoloF (black traces in Fig. 5a–d) showed a main minimum at ~1656 cm^{-1} at all tested conditions, attributed to α-helix moieties, suggesting that the protein is in its native structure. It is therefore possible to state that the folding of Chry adsorbed HoloF does not significantly change at the diverse tested conditions, both above the isoelectric point of HoloF (pI 4.1–5.1). In more detail, at phagosome ionic strength, for both acidic and neutral pH (See Fig. 5a and **b** respectively), the secondary structure of HoloF was minimally affected: a broad and weak shoulder in the 1640-1620 cm^{-1} spectral region may be appreciated. This shoulder had two local minima, at ~1632 and ~1620 cm^{-1}, more easily appreciable at acidic pH for t = 1 week and at neutral pH for t = 2 h and t = 48 h. Whether the local minima at about 1620 cm^{-1} was indicative of a very strong hydrogen bond pattern, undoubtedly attributed to inter-molecular β-structures in protein aggregates, the interpretation of the 1632 cm^{-1} shoulder, and in general of the bands in the 1640-1630 cm^{-1} spectral region, is more controversial. Spectral components in the aforementioned spectral region are

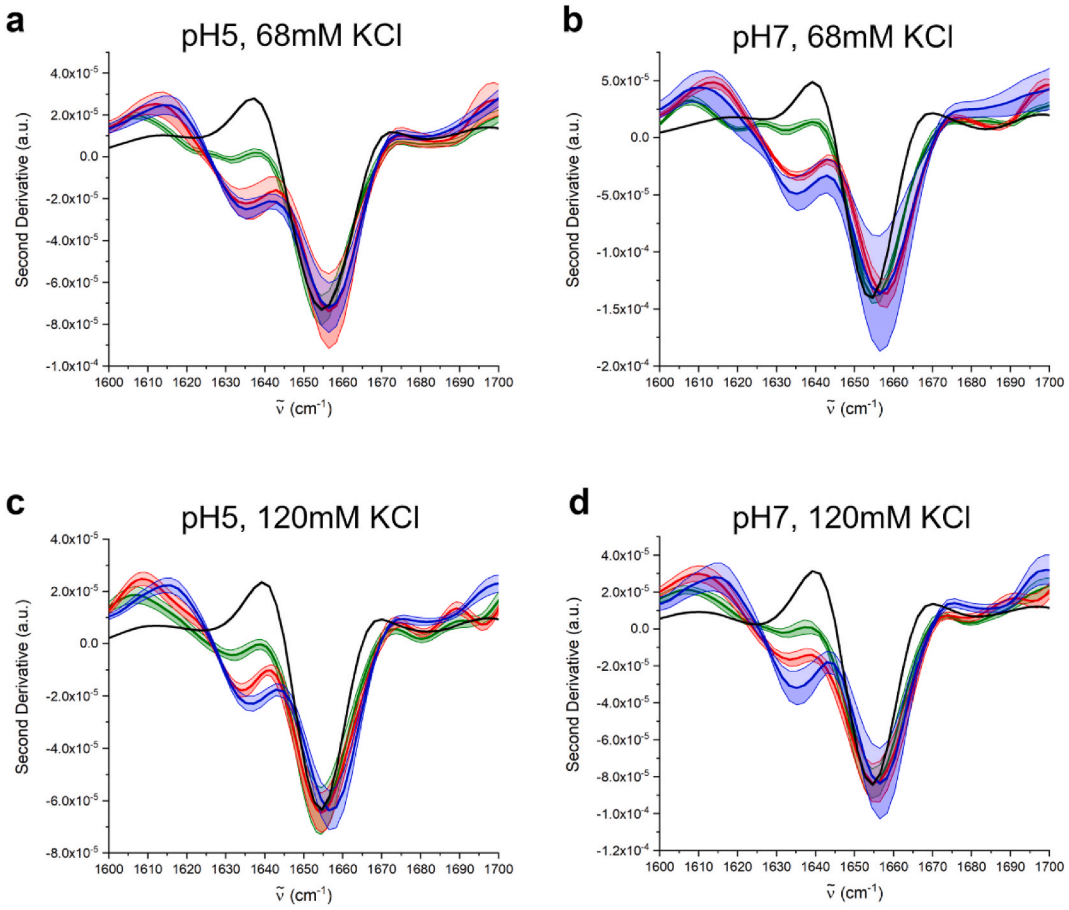

Fig. 6. *Micro-FTIR spectra of AF-Chry adducts*. Second derivative of AF-Chry adduct micro-spectra averaged on fifteen acquisitions at incubation times 2 h (green plot), 48 h (red line) and 1 week (blue line) for the following incubation conditions: **a**) 68 mM KCl, pH 5.0 (phagosomal conditions); **b**) 68 mM KCl, pH 7.0 (phagosomal conditions); **c**) 120 mM KCl, pH 5.0 (cytosolic conditions); **d**) 120 mM KCl, pH 7.0 (cytosolic conditions). Green, red and blue-shadowed regions represent the spectral standard deviation at each considered incubation time. AF second derivative ATR-FTIR spectrum is also plotted for each pH and ionic strength (black line). Data are normalized at main peak. The rearrangements of ApoF loaded on Chry, when compared to pristine ApoF, are more severe, than those of HoloF-Chry. This finding suggests a proper misfolding only in the case ApoF. For more details see text.

usually assigned either to native β-sheets or considered indicative of new β-strands or turns in monomeric partially folded intermediates of protein misfolding, but also in oligomers or aggregates, both amorphous and fibrillar ones [68]. Given the interpretative constraints imposed by the standard deviation of the spectra, for the system under analysis, taken into consideration that the spectral component at about 1632 cm^{-1} cannot be distinguished in the untreated HoloF, it can be concluded that, at both acidic and neutral phagosome conditions, HoloF loaded on Chry tends to rearrange to a partially folded monomeric intermediate, inclined to aggregate. A very similar consideration may be drawn out for HoloF-Chry adducts at physiological and non-physiological cytosol conditions (Fig. 5c and d respectively), with the difference being that at slightly acidic pH and cytosolic ionic strength (see Fig. 5c), only the spectral component at ~1632 cm^{-1} stably shows up in second derivative analysis (see Fig. 5d). Overall, it is possible to appreciate a relatively moderate standard deviation of the second derivative spectra, and in particular of its α-helix contribution, as well as the stability in position of the α-helix peak, indicative of the fact that the helix pattern of HoloF is quite well preserved for all tested conditions. It is however interesting to highlight that for those conditions where the α-helix component variability was greater (*e.g.* KCl 120 mM, pH 5.0, 48 h and KCl 120 mM, pH 7.0, 1 week), a shoulder at ~1688 cm^{-1} appeared, diagnostic of extended β-turns and loops possibly formed as a consequence of a partial α-helix misfolding [69]. The collected experimental evidence, including the lack of any clear time-dependent trend, led us to postulate that the interplay between pH and ionic strength plays the crucial role for the structural stability of HoloF loaded onto Chry.

When considering ApoF, the behavior of the native protein was fully similar to HoloF: second derivative spectra of pristine ApoF in all tested conditions exhibited a prominent peak in the α-helix region, centered at ~1656 cm^{-1} (See Fig. 6a–d, black plots). At a first glance, Fig. 6 shows more pronounced second derivative variation of ApoF loaded onto Chry with respect to HoloF loaded onto the same fiber. In particular, the ApoF-Chry adduct exibited a comparable time-dependent trend in phagosome condition at both pH 5.0 and pH 7.0, as shown respectively in Fig. 6 panels a and **b**. After 2 h incubation (green line), two shoulders of the main α -helix peak, at 1656 cm^{-1} were detected, centered respectively at ~1632 and below 1620 cm^{-1}. Over time, the second derivative analysis highlighted the prevalence of the spectral component centered at 1632 cm^{-1} and its shift toward higher wavenumbers (about 1635 cm^{-1}). At 48 h (red line) and 1 week (blue line) incubation time, the behavior of ApoF on Chry fiber at cytosolic conditions for both acidic and neutral pH was fully comparable (Fig.6 panel c and d), while the spectral component at 1620 cm^{-1} at 2 h was suppressed in ApoF and only the component at 1632 cm^{-1} could be detected.

Taking into consideration the spectral interpretation of the aforementioned components, already provided when describing HoloF-Chry adducts, the monitored trend suggests the partial misfolding of ApoF, first associated with the transient formation of intermolecular aggregates as a consequence of new β-strands or turns, and then with the stable settle of oligomeric aggregates characterized by weaker hydrogen-bonded structures, as proven by the red-shift of β-structures from 1632 to 1635 cm^{-1} [70].

To sum up, micro-FTIR analysis indicated that the rearrangements undergone by ApoF are more severe than the ones undergone by HoloF upon interaction with Chry fibers, letting us speculate about a proper protein misfolding only in the case of ApoF. It is possible to conclude that the interaction with Chry fibers primarily induces misfolding of ferritin when the protein is iron-free, suggesting that iron-loading, despite allowing a deeper interaction with the fiber as proven by IR nanoscopy, assures more stability to the protein against the unfolding effect of asbestos.

Eucaryotic ferritin has a highly conserved three-dimensional structure, composed of 24 subunits of two types, heavy (H, 21 KD 178 residues) and light (L, 19 KD 174 residues) chains. Its secondary structure is mainly composed (41–70 %) of alfa-helices [60,71,72]. They co-assemble to form an almost spherical nanocage with inner and outer diameters of 8 nm and 12 nm, respectively. The ferritin nanocage is comprised of six hydrophobic channels belonging to alfa-helix D, and eight narrow hydrophilic channels belonging to alfa-helix E, which represent pores for iron ions in both H and L subunits. Importantly, the resulting nanocage is very stable between pH 3 and 9 [70]. The ferroxidase center is buried inside the alfa-helices of the H subunit, and is accessible from the hydrophilic channels. The L-subunits facilitate iron hydrolysis and mineralization. From these data, it is argued that alfa-helix folding is a key factor for ferritin-mediated iron uptake, oxidation and core formation, and that changes of the secondary structure are expected to result in an important functional loss.

Although we did not prove that the misfolding induced by adduct formation determines a loss of ferritin function, it is likely that this is the case. Furthermore, in view of the results obtained from the nanoscale analysis, and verification of the major structural stability of HoloF with respect to ApoF at every tested condition, it is also plausible to state that HoloF is able to retain its iron storage function following interaction with the asbestos fiber, even if it may lose its capacity for releasing iron. Conversely, ApoF is probably no longer able to exert its physiological functions.

The secondary structure of ApoF was also investigated by ATR-FTIR in the supernatant of ApoF-Chry adducts. Fig. 4S shows the second derivative spectra of this supernatant in phagosome and cytosolic conditions, incubated with Chry for 48 h. The spectra are very similar, characterized by the main peak in the region of the α-helix (1656 cm^{-1}) as native ApoF, for all tested condition. These additional data are in line with fact the free ApoF maintains its ferroxidase activity upon Chry interaction [44] and essentially confirms the structure-activity relationship paradigm.

Ferritins possess other important functions besides iron storage. Among these, regulation of protein translation, apoptosis, and chemokine receptor signaling are included [71,73]. The effects of ferritin-Chry interaction on each specific function at cellular level deserve to be investigated and will be a next target of our research. Nevertheless, it is worthy of note that the exposure of cell cultures to asbestos fibers (Chry included) results in a significant new synthesis of ApoF [45,46], which was suggested to be a cell reaction mechanism of defense against the ROS production catalyzed by the ingested fibers [46]. The novel finding described in this paper, that cellular asbestos fiber interaction may affect both the structure and the function of the interacting ferritins, suggests another more complex scenario.

Cytosolic fibers can sequester iron (III) directly [74] from the labile iron pool (LIP). LIP consists of both forms of ionic iron (Fe^{2+}

and Fe^{3+}) complexed by diverse low-molecular weight organic chelators with low affinity to iron ions, such as citrate, phosphate and other organic ions. Whenever cell iron availability is impaired, Iron Regulatory Proteins (IRPs) sense it and stimulate iron uptake via DMT1 and the transferrin receptor (TfR) expression, as shown by Ghio et al. in lung tissue of patients with asbestosis [50] and in cell cultures [47,48]. As described in different cell types [45,46], upon iron uptake initiation, LIP reaches a high level, and, as a response, new ApoF synthesis is triggered. In the cytosol (neutral pH), the fibers can meet either ApoF (newly synthetized) or HoloF. The findings presented here highlight that the ApoF-Chry interaction induces a change in ApoF secondary structure, which very likely compromises its ferroxidase activity. As a consequence, the oxidation of imported iron (II) will be impaired, HoloF concentration is expected to decrease, while LIP increases. At the same time, Chry fibers themselves can promote iron oxidation [44], competing with the residual ferroxidase activity of unbounded ApoF and inhibiting the iron loading in the ferritin cage, thus contributing to an increase in the labile iron (III) pool and further reducing HoloF concentration. We put forward the hypothesis that the structural changes we found in ApoF, together with the low level of HoloF concentration, inhibits the negative feedback signal for switching-off iron import mechanisms, while still allowing ApoF synthesis. We think it possible that this failure, which in experimental models is induced by the repression of ApoF synthesis [75], could also be induced by the strong structural changes caused in ApoF by Chry, together with the decrease of HoloF, a situation which could resemble what was reported by Kakhlon and Cabantchik [75], who showed that inhibiting ferritin expression allows a significant increase of LIP, escaping IRPs sensing. The overall result may be that a persistent iron import is maintained and iron overload is eventually established.

In the phago-lysosomal, as well as in the auto-phagosomal compartment, the interaction between HoloF and asbestos fibers is also possible [76]. Considering the strong binding of HoloF in the HoloF-Chry adduct, we speculate that the high affinity of the fiber for the iron-loaded protein, despite it failing to modify significantly its secondary structure, may inhibit the Fe(III) release from it, making more severe the iron request and initiate asbestos body formation on longer fibers [77]. The global paradoxical result of this scenario is an increased request for iron from the outside, together with a persistent iron overload, already reported by other authors [47,48,50]. Altogether, continuous new ApoF synthesis, its continuous structural and functional modification by the fibers, the continuous iron uptake and the persistent iron overload, may create a perfect basis for the generation of neoplastic cells. Interestingly, treatment with either ferric nitrilotriacetate, a cell-permeating iron complex (causing an intracellular overloading of iron), or iron-free synthetic Chry does not exert any of the cytotoxic effects induced by natural Chry or by iron-loaded synthetic Chry. This suggests that Chry is not toxic by acting simply as a carrier of iron into the cell [43,78]. Another key player could be the Chry-induced modification of ferritins.

4. Conclusions

Previous work showed that adsorption on asbestos induces structural changes in the bound protein. These works dealt mainly with the quality of the protein structure (mainly serum albumin), independently on any relation with asbestos-related diseases. For the first time, we focused our attention on the interaction between asbestos fibers and ferritin, a protein involved in iron metabolism, which is strongly modified in asbestos-related diseases. Moreover, for this purpose, High Resolution Transmission Electron Microscopy (HR-TEM) was employed together with FTIR microspectroscopy and Infrared nanoscopy, which to the best of our knowledge, have not been used up to now for this purpose.

The objectives of this study were firstly to define the features of ferritin adsorption to different asbestos fibers (serpentine and amphiboles) and secondly to investigate the effect of this adsorption on protein structure. We show here that the amount of ferritin bound to different asbestos fibers falls within the range of 0.011–0.150 μg protein/μg fibers. Chry showed the maximal affinity for HoloF with respect to Croc and Amo. On this basis, we decided to study in more detail, the features of Ferritin-Chry adsorption and its effects on the protein structure. The interaction was rapid, reaching ~80 % of the maximum value after 10 min of incubation at RT. The extent of ferritin adsorption was comparable (non-significantly different) at the different pHs which can be found by the fiber in the cell interior. If actively ingested, the fiber finds either a neutral pH (phagosomal early) or an acidic pH 5.0 (phagosomal late). If it reaches the cell interior by membrane-piercing, it finds a neutral pH (7.0 cytosolic). Very interestingly, ApoF showed a different pattern of adsorption. It was significantly lower with respect to HoloF at the pHs tested. Its maximum binding was found at pH 7.0. These different patterns of binding could suggest that iron-loaded ferritin could be bound to the fiber in the cytosol and in the phagosomal compartment, while ApoF is expected to be mainly bound in the cytosolic compartment, where it can meet the fiber, just when newly-synthetized. The lower extent of interaction of ApoF with Chry suggests that the presence of iron could improve the interaction. This possibility was confirmed by saturating Chry fibers with ferric iron before the incubation with HoloF. Under this condition, the extent of ferritin adsorption was strongly inhibited, suggesting the hypothesis that the mechanism of adsorption could rely on iron sequestration by the fibers from the protein. This mechanism could also explain the lower adsorption affinity of ferritin for Croc and Amo, amphiboles which are richer in iron with respect to Chry. The ultrastructural appearance of the HoloF- and ApoF-Chry adducts revealed that either HoloF or ApoF mainly showed a homogeneous pattern of distribution on the fibers. However, frequently, they appeared as a bulge, suggesting a different extent of binding at specific sites of the fiber. Nano-IR analysis confirmed that the protein, in either case (HoloF and ApoF), homogenously decorates the fiber, which excludes a non-specific trapping of the proteins, and further reveals a different mechanism of binding of the two isoforms. Despite accessing the same binding sites, HoloF and ApoF may interact differently with the fiber, contributing to explain their penetration capacity and potential impact on their structure. Again, the presence of iron induces a more intimate interaction and may possibly affect the fiber structure. The FTIR spectroscopic study showed that the interaction with Chry fibers primarily induces misfolding of ferritins when the protein is iron-free, suggesting that iron loading insures more stability to the protein. The final stages of the misfolded state exhibit similar structural features, with a fraction of the peptide backbone adopting a β-sheet conformation. The rearrangements in beta-sheet twist angles during the misfolding process were more evident for the cytosolic conditions. α -helix folding is a key factor for ferritin-mediated iron uptake, iron oxidation and core

formation, and changes of its secondary structure are expected to result in an important functional loss. Although we did not prove that misfolding induced by adduct formation determines a loss of ferritin function and contributes to iron overload, it is likely that this is the case. These considerations, which clearly represent a limitation of the paper, will represent the aim of our next paper. Furthermore, in view of the results obtained from the nanoscale analysis, and verification of the major structural stability of HoloF with respect to ApoF at every tested condition, it is also plausible to state that HoloF is able to retain its iron storage function following interaction with the asbestos fiber, even if it may lose its capacity to release iron, while ApoF is presumed to be no longer able to exert its physiological functions.

Ferritins possess other functions besides iron storage. Among these, regulation of protein translation, apoptosis and chemokine receptor signaling are included. The effects of Chry interaction on these functions within the cell environment deserve further investigation and will be the next target of our research. An example of this general principle is the activity of carbon nanotubes which after adsorption of either hemoglobin or transferrin, acquire a significantly aggravated cytotoxicity to mesothelial cells, with an increase in cellular catalytic ferrous iron and DNA damage also observed [79]. In conclusion, our findings reveal a new potential toxic activity of asbestos fibers: they bind to proteins and may modify their function as a result. This capacity, particularly in relation to ferritin, may be very likely one of the causal events leading to changes of iron homeostasis, iron overload and lung inflammation. An in-depth biophysical characterization of the adsorption phenomena is under study.

Funding

IR s-SNOM imaging and HR-TEM analyses were carried out through CERIC-ERIC research infrastructure at SISSI beamline (Elettra Sincrotrone Trieste) and at National Institute of Materials Physics (NIMP, Romania) during two allocated beamtimes (n° proposals: 20227247 and 20217169); Regione Friuli Venezia Giulia (Contributi alle Aziende Sanitarie per la realizzazione di progetti di ricerca sulle malattie correlabili all'amianto, decreto n. 2100/SP dd. 2/11/20). C. R. acknowledges the financial support from the Ministry of Research, Innovation and Digitization, Romania, through the Core Project PC1-PN23080101.

CRediT authorship contribution statement

Martina Zangari: Data curation, Formal analysis, Investigation, Methodology, Validation. **Federica Piccirilli:** Formal analysis, Investigation, Methodology, Validation, Writing – original draft, Writing – review & editing. **Lisa Vaccari:** Conceptualization, Funding acquisition, Investigation, Methodology, Resources, Supervision, Visualization, Writing – original draft, Writing – review & editing. **Cristian Radu:** Investigation, Validation. **Paola Zacchi:** Investigation, Validation. **Annalisa Bernareggi:** Funding acquisition, Writing – original draft, Writing – review & editing. **Sara Leone:** Methodology. **Giuliano Zabucchi:** Conceptualization, Investigation, Methodology, Project administration, Supervision, Visualization, Writing – original draft, Writing – review & editing. **Violetta Borelli:** Resources, Writing – review & editing.

Declaration of competing interest

The authors declare that they have no known competing financial interests or personal relationships that could have appeared to influence the work reported in this paper.

Acknowledgements

We would like to hank Dr Diana Bedolla for her support in sample preparation. We thank CERIC-ERIC (Central European Research Infrastructure Consortium) for supporting the doctoral fellowship to M. Z. IR nanoscopic analysis was partly performed within the framework of the Nanoscience Foundry and Fine Analysis (NFFA-MIUR Italy) facility. We also thank Dr Andrew Constanti (UCL School of Pharmacy, UK) for reading the manuscript.

Appendix A. Supplementary data

Supplementary data to this article can be found online at https://doi.org/10.1016/j.heliyon.2024.e38966.

References

[1] E. Hiriart, R. Deepe, A. Wessels, Mesothelium and malignant mesothelioma, J. Dev. Biol. 7 (2) (2019) 7, https://doi.org/10.3390/jdb7020007.
[2] G. Gaudino, J. Xue, H. Yang, How asbestos and other fibers Cause mesothelioma, Transl. Lung Cancer Res. 9 (Suppl 1) (2020) S39–S46, https://doi.org/10.21037/tlcr.2020.02.01.
[3] F. Delva, P. Andujar, A. Lacourt, P. Brochard, J.-C. Pairon, [Occupational risk factors for lung cancer], Rev. Mal. Respir. 33 (6) (2016) 444–459, https://doi.org/10.1016/j.rmr.2015.10.003.
[4] C. Gilham, C. Rake, G. Burdett, A.G. Nicholson, L. Davison, A. Franchini, J. Carpenter, J. Hodgson, A. Darnton, J. Peto, Pleural mesothelioma and lung cancer Risks in relation to Occupational history and asbestos lung Burden, Occup. Environ. Med. 73 (5) (2016) 290–299, https://doi.org/10.1136/oemed-2015-103074.

[5] R.A. Lemen, Mesothelioma from asbestos exposures: Epidemiologic patterns and impact in the United States, J. Toxicol. Environ. Health B Crit. Rev. 19 (5–6) (2016) 250–265, https://doi.org/10.1080/10937404.2016.1195323.
[6] D.W. Kamp, S.A. Weitzman, The molecular basis of asbestos induced lung injury, Thorax 54 (7) (1999) 638–652, https://doi.org/10.1136/thx.54.7.638.
[7] B.T. Mossman, In vitro studies on the biologic effects of fibers: Correlation with in vivo Bioassays, Environ. Health Perspect. 88 (1990) 319–322, https://doi.org/10.1289/ehp.9088319.
[8] G. Liu, P. Cheresh, D.W. Kamp, Molecular basis of asbestos-induced lung disease, Annu. Rev. Pathol. 8 (2013) 161–187, https://doi.org/10.1146/annurev-pathol-020712-163942.
[9] A. Bloise, C. Ricchiuti, R. Punturo, D. Pereira, Potentially toxic Elements (PTEs) associated with asbestos chrysotile, Tremolite and Actinolite in the Calabria region (Italy), Chem. Geol. 558 (2020) 119896, https://doi.org/10.1016/j.chemgeo.2020.119896.
[10] V. Borelli, E. Trevisan, F. Vita, G. Zabucchi, The Secretory response of Rat Peritoneal Mast cells on exposure to mineral fibers, Int. J. Environ. Res. Publ. Health 15 (1) (2018) 104, https://doi.org/10.3390/ijerph15010104.
[11] J.M.G. Davis, Further observations on the ultrastructure and Chemistry of the formation of asbestos bodies, Exp. Mol. Pathol. 13 (3) (1970) 346–358, https://doi.org/10.1016/0014-4800(70)90096-1.
[12] W. Malorni, F. Iosi, M. Falchi, G. Donelli, On the mechanism of cell Internalization of chrysotile fibers: an Immunocytochemical and ultrastructural study, Environ. Res. 52 (2) (1990) 164–177, https://doi.org/10.1016/s0013-9351(05)80251-8.
[13] W. Liu, J.D. Ernst, V.C. Broaddus, Phagocytosis of crocidolite asbestos induces oxidative stress, DNA damage, and apoptosis in mesothelial cells, Am. J. Respir. Cell Mol. Biol. 23 (3) (2000) 371–378, https://doi.org/10.1165/ajrcmb.23.3.4094.
[14] H. Nagai, S. Toyokuni, Differences and Similarities between carbon nanotubes and asbestos fibers during mesothelial Carcinogenesis: Shedding light on fiber Entry mechanism, Cancer Sci. 103 (8) (2012) 1378–1390, https://doi.org/10.1111/j.1349-7006.2012.02326.x.
[15] L. Andolfi, E. Trevisan, M. Zweyer, S. Prato, B. Troian, F. Vita, V. Borelli, M.R. Soranzo, M. Melato, G. Zabucchi, The crocidolite Fibres interaction with Human mesothelial cells as investigated by combining electron microscopy, atomic Force and scanning near-field optical microscopy, J. Microsc. 249 (3) (2013) 173–183, https://doi.org/10.1111/jmi.12006.
[16] B.W. Case, J.L. Abraham, G. Meeker, F.D. Pooley, K.E. Pinkerton, Applying Definitions of “asbestos” to environmental and “Low-dose” exposure levels and Health effects, particularly malignant mesothelioma, J. Toxicol. Environ. Health B Crit. Rev. 14 (1–4) (2011) 3–39, https://doi.org/10.1080/10937404.2011.556045.
[17] P. Ballirano, A. Bloise, A.F. Gualtieri, M. Lezzerini, A. Pacella, N. Perchiazzi, M. Dogan, A.U. Dogan, Mineral fibers: crystal Chemistry, Chemical-Physical Properties, Biological Interaction and Toxicity 18 (2017) 17–64, https://doi.org/10.1180/EMU-notes.18.2. European Mineralogical Union.
[18] F. Valerio, D. Balducci, L. Scarabelli, Selective adsorption of serum proteins by chrysotile and crocidolite, Environ. Res. 41 (2) (1986) 432–439, https://doi.org/10.1016/S0013-9351(86)80137-2.
[19] M. Kucki, J.-P. Kaiser, M. Clift, B. Rothen-Rutishauser, A. Fink, P. Wick, The role of the protein Corona in fiber structure-activity relationships, Fibers 2 (2014) 187–210, https://doi.org/10.3390/fib2030187.
[20] H. Nagai, T. Ishihara, W.-H. Lee, H. Ohara, Y. Okazaki, K. Okawa, S. Toyokuni, Asbestos surface Provides a Niche for oxidative modification, Cancer Sci. 102 (12) (2011) 2118–2125, https://doi.org/10.1111/j.1349-7006.2011.02087.x.
[21] R. Dumitru-Stănescu, C. Mandravel, C. Bercu, Infrared and Nuclear Magnetic Resonance studies of some surface properties of asbestos–albumin interactions, Analyst 119 (4) (1994) 689–691, https://doi.org/10.1039/AN9941900689.
[22] A. Adamiano, I.G. Lesci, D. Fabbri, N. Roveri, Adsorption of bovine serum albumin onto synthetic Fe-doped Geomimetic chrysotile, J. R. Soc. Interface 12 (107) (2015) 20150186, https://doi.org/10.1098/rsif.2015.0186.
[23] R. Artali, A. Del Pra, E. Foresti, I.G. Lesci, N. Roveri, P. Sabatino, Adsorption of Human serum albumin on the chrysotile surface: a molecular Dynamics and spectroscopic investigation, J. R. Soc. Interface 5 (20) (2008) 273–283, https://doi.org/10.1098/rsif.2007.1137.
[24] G. Falini, E. Foresti, I.G. Lesci, B. Lunelli, P. Sabatino, N. Roveri, Interaction of bovine serum albumin with chrysotile: spectroscopic and morphological studies, Chemistry 12 (7) (2006) 1968–1974, https://doi.org/10.1002/chem.200500709.
[25] B. Fubini, F. Barceló, C. Otero Areán, Ferritin adsorption on amosite fibers: possible Implications in the formation and toxicity of asbestos bodies, J. Toxicol. Environ. Health 52 (4) (1997) 343–352, https://doi.org/10.1080/00984109708984069.
[26] V.L. Roggli, V.L. Roggli, T.D. Oury, T.A. Sporn, Pathology of Asbestos-Associated Diseases, Springer, New York, 2004.
[27] N.B. Gandolfi, A.F. Gualtieri, S. Pollastri, E. Tibaldi, F. Belpoggi, Assessment of asbestos body formation by high resolution FEG–SEM after exposure of Sprague–Dawley Rats to chrysotile, crocidolite, or Erionite, J. Hazard Mater. 306 (2016) 95–104, https://doi.org/10.1016/j.jhazmat.2015.11.050.
[28] A.M. Churg, M.L. Warnock, Asbestos and other ferruginous bodies: their formation and Clinical significance, Am. J. Pathol. 102 (3) (1981) 447–456.
[29] Agency for toxic Substances and disease Registry. https://www.atsdr.cdc.gov/index.html. (Accessed 14 June 2024).
[30] T.L. McLemore, M.L. Mace, V. Roggli, M.V. Marshall, E.C. Lawrence, R.K. Wilson, R.R. Martin, B.R. Brinkley, S.D. Greenberg, Asbestos body Phagocytosis by Human free Alveolar macrophages, Cancer Lett. 9 (2) (1980) 85–93, https://doi.org/10.1016/0304-3835(80)90111-1.
[31] V. Borelli, M. Zangari, A. Bernareggi, F. Bardelli, F. Vita, G. Zabucchi, Ferruginous bodies exert a strong Proinflammatory effect, J. Toxicol. Environ. Health 86 (8) (2023) 241–245, https://doi.org/10.1080/15287394.2023.2181899.
[32] A.J. Ghio, A. Churg, V.L. Roggli, Ferruginous bodies: Implications in the mechanism of fiber and Particle toxicity, Toxicol. Pathol. 32 (6) (2004) 643–649, https://doi.org/10.1080/01926230490885733.
[33] V. Borelli, C. Brochetta, M. Melato, C. Rizzardi, M. Polentarutti, C. Busatto, F. Vita, R. Abbate, R. Gotter, G. Zabucchi, A procedure for the isolation of asbestos bodies from lung tissue by exploiting their Magnetic properties: a new approach to asbestos body study, J. Toxicol. Environ. Health 70 (14) (2007) 1232–1240, https://doi.org/10.1080/15287390701380906.
[34] M. Governa, M. Amati, S. Fontana, I. Visona, null, G.C. Botta, F. Mollo, D. Bellis, P. Bo, Role of iron in asbestos-body-induced oxidant Radical generation, J. Toxicol. Environ. Health 58 (5) (1999) 279–287, https://doi.org/10.1080/009841099157241.
[35] B. Fubini, L. Mollo, Role of iron in the Reactivity of mineral fibers, Toxicol. Lett. 82–83 (1995) 951–960, https://doi.org/10.1016/0378-4274(95)03531-1.
[36] L.G. Lund, A.E. Aust, Iron mobilization from asbestos by chelators and ascorbic Acid, Arch. Biochem. Biophys. 278 (1) (1990) 61–64, https://doi.org/10.1016/0003-9861(90)90231-m.
[37] P.S. Gilmour, D.M. Brown, P.H. Beswick, W. MacNee, I. Rahman, K. Donaldson, Free Radical activity of Industrial fibers: role of iron in oxidative stress and Activation of Transcription factors, Environ. Health Perspect. 105 (1997) 1313–1317, https://doi.org/10.2307/3433553.
[38] A.F. Gualtieri, G. Lusvardi, A. Zoboli, D. Di Giuseppe, M. Lassinantti Gualtieri, Biodurability and release of metals during the Dissolution of chrysotile, crocidolite and fibrous Erionite, Environ. Res. 171 (2019) 550–557, https://doi.org/10.1016/j.envres.2019.01.011.
[39] Z. Shen, D. Bosbach, M.F. Hochella, D.L. Bish, M.G. Williams, R.F. Dodson, A.E. Aust, Using in vitro iron Deposition on asbestos to model asbestos bodies formed in Human lung, Chem. Res. Toxicol. 13 (9) (2000) 913–921, https://doi.org/10.1021/tx000025b.
[40] F. Bardelli, G. Veronesi, S. Capella, D. Bellis, L. Charlet, A. Cedola, E. Belluso, New Insights on the Biomineralisation process developing in Human lungs around inhaled asbestos Fibres, Sci. Rep. 7 (2017) 44862, https://doi.org/10.1038/srep44862.
[41] L. Pascolo, V. Borelli, V. Canzonieri, A. Gianoncelli, G. Birarda, D.E. Bedolla, M. Salomé, L. Vaccari, C. Calligaro, M. Cotte, B. Hesse, F. Luisi, G. Zabucchi, M. Melato, C. Rizzardi, Differential protein folding and chemical changes in lung tissues exposed to asbestos or Particulates, Sci. Rep. 5 (2015) 12129, https://doi.org/10.1038/srep12129.
[42] J.A. Hardy, A.E. Aust, The effect of iron binding on the Ability of crocidolite asbestos to Catalyze DNA single-Strand Breaks, Carcinogenesis 16 (2) (1995), https://doi.org/10.1093/carcin/16.2.319.
[43] E. Gazzano, F. Turci, E. Foresti, M.G. Putzu, E. Aldieri, F. Silvagno, I.G. Lesci, M. Tomatis, C. Riganti, C. Romano, B. Fubini, N. Roveri, D. Ghigo, Iron-loaded synthetic chrysotile: a new model solid for studying the role of iron in asbestos toxicity, Chem. Res. Toxicol. 20 (3) (2007) 380–387, https://doi.org/10.1021/tx600354f.

[44] M. Zangari, V. Borelli, A. Bernareggi, G. Zabucchi, Asbestos fibers promote iron oxidation and Compete with apoferritin enzymatic activity, J. Toxicol. Environ. Health 86 (2–3) (2023) 69–73, https://doi.org/10.1080/15287394.2022.2164391.
[45] R. Fang, A.E. Aust, Induction of ferritin synthesis in Human lung Epithelial cells treated with crocidolite asbestos, Arch. Biochem. Biophys. 340 (2) (1997) 369–375, https://doi.org/10.1006/abbi.1997.9892.
[46] W. Aung, S. Hasegawa, T. Furukawa, T. Saga, Potential role of ferritin heavy Chain in oxidative stress and apoptosis in Human mesothelial and mesothelioma cells: Implications for asbestos-induced Oncogenesis, Carcinogenesis 28 (9) (2007) 2047–2052, https://doi.org/10.1093/carcin/bgm090.
[47] A.J. Ghio, J.M. Soukup, L.A. Dailey, J.H. Richards, H. Tong, The biological effect of asbestos exposure is dependent on changes in iron homeostasis, Inhal. Toxicol. 28 (14) (2016) 698–705, https://doi.org/10.1080/08958378.2016.1257665.
[48] A. Ghio, R.J. Tan, K. Ghio, C.L. Fattman, T.D. Oury, Iron accumulation and expression of iron-related proteins following Murine exposure to crocidolite, J. Environ. Pathol. Toxicol. Oncol. 28 (2) (2009) 153–162, https://doi.org/10.1615/jenvironpatholtoxicoloncol.v28.i2.70.
[49] X. Wang, Y. Wu, J.G. Stonehuerner, L.A. Dailey, J.D. Richards, I. Jaspers, C.A. Piantadosi, A.J. Ghio, Oxidant generation promotes iron sequestration in BEAS-2B cells exposed to asbestos, Am. J. Respir. Cell Mol. Biol. 34 (3) (2006) 286–292, https://doi.org/10.1165/rcmb.2004-0275OC.
[50] A.J. Ghio, E.N. Pavlisko, V.L. Roggli, Iron and iron-related proteins in asbestosis, J. Environ. Pathol. Toxicol. Oncol. 34 (4) (2015) 277–285, https://doi.org/10.1615/jenvironpatholtoxicoloncol.2015013397.
[51] N. Kohyama, Y. Shinohara, Y. Suzuki, Mineral phases and some Reexamined characteristics of the International union against cancer standard asbestos samples, Am. J. Ind. Med. 30 (5) (1996) 515–528, https://doi.org/10.1002/(SICI)1097-0274(199611)30:5<515::AID-AJIM1>3.0.CO;2-S.
[52] J. Canton, R. Khezri, M. Glogauer, S. Grinstein, Contrasting phagosome pH regulation and Maturation in Human M1 and M2 macrophages, Mol. Biol. Cell 25 (21) (2014) 3330–3341, https://doi.org/10.1091/mbc.E14-05-0967.
[53] C. Ince, B. Thio, B. Van Duijn, J.T. Van Dissel, D.L. Ypey, P.C.J. Leijh, Intracellular K+, Na+ and Cl− concentrations and membrane potential in Human Moncytes, Biochim. Biophys. Acta Biomembr. 905 (1) (1987) 195–204, https://doi.org/10.1016/0005-2736(87)90023-X.
[54] J.M. Heiple, D.L. pH. Taylor, Changes in Pinosomes and phagosomes in the Ameba, Chaos Carolinensis, J. Cell Biol. 94 (1) (1982) 143–149, https://doi.org/10.1083/jcb.94.1.143.
[55] G. Birarda, D. Bedolla, F. Piccirilli, C. Stani, H. Vondracek, L. Vaccari, Chemical analyses at micro and nano Scale at SISSI-Bio beamline at Elettra-Sincrotrone Trieste, in: Biomedical Vibrational Spectroscopy 2022: Advances in Research and Industry, vol. 11957, SPIE, 2022, pp. 27–39, https://doi.org/10.1117/12.2607751.
[56] F. Piccirilli, G. Schirò, V. Vetri, S. Lupi, A. Perucchi, V. Militello, Decoding vibrational states of Concanavalin A Amyloid Fibrils, Biophys. Chem. 199 (2015) 17–24, https://doi.org/10.1016/j.bpc.2015.02.007.
[57] A. Barth, Infrared spectroscopy of proteins, Biochim. Biophys. Acta 1767 (9) (2007) 1073–1101, https://doi.org/10.1016/j.bbabio.2007.06.004.
[58] F. Piccirilli, F. Tardani, A. D'Arco, G. Birarda, L. Vaccari, S. Sennato, S. Casciardi, S. Lupi, Infrared Nanospectroscopy reveals DNA structural modifications upon Immobilization onto Clay nanotubes, Nanomaterials 11 (5) (2021) 1103, https://doi.org/10.3390/nano11051103.
[59] T. Taubner, F. Keilmann, R. Hillenbrand, Nanoscale-Resolved Subsurface Imaging by Scattering-type Near-Field Optical Microscopy, 2005.
[60] A. Caldiroli, S. Cappelletti, G. Birarda, A. Redaelli, S.A. Riboldi, C. Stani, L. Vaccari, F. Piccirilli, Infrared Nanospectroscopy depth-dependent study of modern materials: Morpho-chemical analysis of Polyurethane/Fibroin binary Meshes, Analyst 148 (15) (2023) 3584–3593, https://doi.org/10.1039/D3AN00336A.
[61] M. Plays, S. Müller, R. Rodriguez, Chemistry and biology of ferritin. Metallomics 2021 13 (5) (2021). https://doi.org/10.1093/mtomcs/mfab021.
[62] F. Valerio, D. Balducci, A. Lazzarotto, Adsorption of proteins by chrysotile and crocidolite: role of molecular weight and charge density 44 (2) (1987) 31–320. https://doi.org/10.1016/S0013-9351(87)80240-2).
[63] N.D. Chasteen, P.M. Harrison, Mineralization in ferritin: an efficient means of iron storage, J. Struct. Biol. 126 (3) (1999) 182–194. https://doi.org/10.1006/jsbi.1999.4118.
[64] N. Jian, M. Dowle, R.D. Horniblow, C. Tselepis, R.E. Palmer, Morphology of the ferritin iron core by aberration corrected scanning transmission electron microscopy, Nanotechnology 27 (46) (2016) 46LT02. https://doi.org/10.1088/0957-4484/27/46/46LT02.
[65] F.D. Pooley, Asbestos bodies, their formation, composition and character, Environ. Res. 5 (4) (1972) 363–379. https://doi.org/10.1016/0013-9351(72)90039-4.
[66] K. Uto, K. Yamamoto, N. Kishimoto, M. Muraoka, T. Aoyagi, I. Yamashita, Electrostatic adsorption of ferritin, proteins and nanoparticle conjugate onto the surface of polyelectrolyte multilayers, J. Mater. Chem. 18 (32) (2008) 3876–3884. https://doi.org/10.1039/B807178K.
[67] A. Yousefi, C. Ying, C.D.J. Parmenter, M. Assadipapari, G. Sanderson, Z. Zheng, L. Xu, S. Zargarbashi, G.J. Hickman, R.B. Cousins, C.J. Mellor, M. Mayer, M. Rahmani, Optical monitoring of in situ iron loading into single, native ferritin proteins, Nano Lett 23 (8) (2023) 3251–3258. https://doi.org/10.1021/acs.nanolett.3c00042.
[68] B. Shivu, S. Seshadri, J. Li, K.A. Oberg, V.N. Uversky, A.L. Fink, Distinct β-sheet structure in protein aggregates determined by ATR-FTIR spectroscopy, Biochemistry 52 (31) (2013) 5176–5183. https://doi.org/10.1021/bi400625v.
[69] A. Dong, P. Huang, W.S. Caughey, Protein secondary structures in water from second-derivative amide I infrared spectra, Biochemistry 29 (13) (1990) 3303–3308. https://doi.org/10.1021/bi00465a022.
[70] G. Zandomeneghi, M.R.H. Krebs, M.G. McCammon, M. FTIR Fändrich, Reveals structural differences between native β-sheet proteins and amyloid fibrils, Protein Science 13 (12) (2004) 3314–3321. https://doi.org/10.1110/ps.041024904.
[71] P. Arosio, R. Ingrassia, P. Cavadini, Ferritins: a family of molecules for iron storage, antioxidation and more, Biochim Biophys Acta 1790 (7) (2009) 589–599. https://doi.org/10.1016/j.bbagen.2008.09.004.
[72] G.C. Wood, R.R. Crichton, Optical rotatory dispersion and circular dichroism studies on ferritin and apoferritin, Biochim. Biophys. Acta. 229 (1) (1971) 83–87. https://doi.org/10.1016/0005-2795(71)90321-7.
[73] D. Finazzi, P. Arosio, Biology of ferritin in mammals: an update on iron storage, oxidative damage and neurodegeneration, Arch. Toxicol. 88 (10) (2014) 1787–1802. https://doi.org/10.1007/s00204-014-1329-0.
[74] J.A. Hardy, A.E. Aust, Iron in asbestos chemistry and carcinogenicity, Chem. Rev. 95 (1) (1995) 97–118. https://doi.org/10.1021/cr00033a005.
[75] O. Kakhlon, Z.I. Cabantchik, The labile iron pool: characterization, measurement, and participation in cellular processes1, Free Radical Biology and Medicine 33 (8) (2002) 1037–1046. https://doi.org/10.1016/S0891-5849(02)01006-7.
[76] M. Truman-Rosentsvit, D. Berenbaum, L. Spektor, L.A. Cohen, S. Belizowsky-Moshe, L. Lifshitz, J. Ma, W. Li, E. Kesselman, I. Abutbul-Ionita, D. Danino, L. Gutierrez, H. Li, K. Li, H. Lou, M. Regoni, M. Poli, F. Glaser, T.A. Rouault, E.G. Meyron-Holtz, Ferritin is secreted via 2 distinct nonclassical vesicular pathways, Blood 131 (3) (2018) 342–352. https://doi.org/10.1182/blood-2017-02-768580.
[77] H.K. Koerten, de Bruijn, W.T. Daems, The formation of asbestos bodies by mouse peritoneal macrophages. an In Vitro study, Am J Pathol 137 (1) (1990) 121–134.
[78] L. Jiang, S. Akatsuka, H. Nagai, S.-H. Chew, H. Ohara, Y. Okazaki, Y. Yamashita, Y. Yoshikawa, H. Yasui, K. Ikuta, K. Sasaki, Y. Kohgo, S. Hirano, Y. Shinohara, N. Kohyama, T. Takahashi, S. Toyokuni, Iron overload signature in chrysotile-induced malignant mesothelioma, J. Pathol. 228 (3) (2012) 366–377. https://doi.org/10.1002/path.4075.
[79] Y. Wang, Y. Okazaki, L. Shi, H. Kohda, M. Tanaka, K. Taki, T. Nishioka, T. Hirayama, H. Nagasawa, Y. Yamashita, S. Toyokuni, Role of hemoglobin and transferrin in multi-wall carbon nanotube-induced mesothelial injury and carcinogenesis, Cancer Sci. 107 (3) (2016) 250–257. https://doi.org/10.1111/cas.12865.